operon expression is increased by uncharged $tRNA^{Trp}$. In *B. subtilis*, as described in this article, uncharged $tRNA^{Trp}$ accumulation leads to AT production, and AT inactivates TRAP, leading to antitermination and increased *trp* operon expression. Each of these regulatory mechanisms appears to be effective in regulating *trp* operon expression. The regulatory differences observed presumably reflect evolutionary adjustments of ancestral species in their attempts to optimize gene expression in relation to operon organization and overall metabolism (*1–3*, *16*, *29*).

References and Notes

1. C. Yanofsky, E. Miles, R. Bauerle, K. Kirschner, in *Encyclopedia of Molecular Biology*, T. E. Creighton, Ed. (Wiley, New York, 1999), pp. 2676–2689.
2. D. Henner, C. Yanofsky, in Bacillus subtilis *and Other Gram-Positive Bacteria: Biochemistry, Physiology and Molecular Genetics* A. L. Sonenshein, J. A. Hoch, R. Losick, Eds. [American Society for Microbiology (ASM), Washington, DC, 1993], pp. 269–280.
3. P. Gollnick, P. Babitzke, E. Merino, C. Yanofsky, in Bacillus subtilis *and Its Closest Relatives: From Genes to Cells* A. L. Sonenshein, J. A. Hoch, R. Losick, Eds. (ASM, Washington, DC, in press).
4. J. Otridge, P. Gollnick, *Proc. Natl. Acad. Sci. U.S.A.* **90**, 128 (1993).
5. P. Babitzke, C. Yanofsky, *Proc. Natl. Acad. Sci. U.S.A.* **90**, 133 (1993).
6. A. A. Antson *et al.*, *Nature* **374**, 693 (1995).
7. E. Merino, P. Babitzke, C. Yanofsky, *J. Bacteriol.* **177**, 6362 (1995).
8. P. Babitzke, D. G. Bear, C. Yanofsky, *Proc. Natl. Acad. Sci. U.S.A.* **92**, 7916 (1995).
9. A. A. Antson *et al.*, *Nature* **401**, 235 (1999).
10. H. Shimotsu, M. I. Kuroda, C. Yanofsky, D. J. Henner, *J. Bacteriol.* **166**, 461 (1986).
11. P. Babitzke, J. T. Stults, S. J. Shire, C. Yanofsky, *J. Biol. Chem.* **269**, 16597 (1994).
12. H. Du, R. Tarpey, P. Babitzke, *J. Bacteriol.* **179**, 2582 (1997).
13. W. Steinberg, *J. Bacteriol.* **117**, 1023 (1974).
14. A. I. Lee, J. P. Sarsero, C. Yanofsky, *J. Bacteriol.* **178**, 6518 (1996).
15. J. P. Sarsero, E. Merino, C. Yanofsky, *Proc. Natl. Acad. Sci. U.S.A.* **97**, 2656 (2000).
16. F. J. Grundy, T. M. Henkin, *J. Mol. Biol.* **235**, 798 (1994).
17. P. Stragier, C. Bonamy, C. Karmazyn-Campelli, *Cell* **52**, 697 (1988).
18. Cultures were grown at 37°C overnight in Vogel-Bonner minimal medium containing 0.5% glucose, supplemented with 50 μg/ml of L-phenylalanine in experiments with Δ*mtrB* strains only. These cultures were then subcultured into the same medium in the presence or absence of 50 μg/ml of L-tryptophan and grown to mid-exponential phase at 37°C. IPTG (1 mM) was added to half of each culture, and after 2 hours, cells were collected. β-Galactosidase activity was assayed by using permeabilized cells in duplicate as described by Miller (*19*).
19. J. H. Miller, in *Experiments in Molecular Genetics* (Cold Spring Harbor Laboratory Press, Cold Spring Harbor, NY, 1972), pp. 352–355.
20. A. Valbuzzi, C. Yanofsky, unpublished data.
21. S. Tabor, C. C. Richardson, *Proc. Natl. Acad. Sci. U.S.A.* **82**, 1074 (1985).
22. Washed *E. coli* cells were disrupted by sonication, the supernatant was treated with 1% streptomycin, and the mixture was heated at 80°C for 7 min. The supernatant was fractionated with ammonium sulfate, the 45 to 70% of saturation fraction was collected, dialyzed, and applied to a DEAE-Sephadex A-25 column. Fractions containing AT were pooled, concentrated, dialyzed, and applied to a Sephadex G-75 sizing column. Fractions with pure AT were pooled and concentrated. AT purity was monitored by gel electrophoresis and staining with Coomassie blue. Protein concentrations were determined by the Advance protein assay (Cytoskeleton).
23. A. Szabo, R. Korszun, F. U. Hartl, J. Flanagan, *EMBO J.* **15**, 408 (1996).
24. M. Martinez-Yamout, G. B. Legge, O. Zhang, P. E. Wright, H. J. Dyson, *J. Mol. Biol.* **300**, 805 (2000).
25. Single-letter abbreviations for the amino acid residues are as follows: A, Ala; C, Cys; D, Asp; E, Glu; F, Phe; G, Gly; H, His; I, Ile; K, Lys; L, Leu; M, Met; N, Asn; P, Pro; Q, Gln; R, Arg; S, Ser; T, Thr; V, Val; W, Trp; Y, Tyr; and X, any amino acid.
26. In vitro transcription attenuation assays followed a previously published procedure (*10*). Purified TRAP (340 nM) and/or AT (various concentrations) were preincubated in the presence of 0.5 mM L-tryptophan at 30°C for 5 min, then the remaining ingredients were added and reactions were carried out at 30°C for 30 min. Samples were electrophoresed on a 5% polyacrylamide-7M urea gel. Radiolabeled RNA bands were quantified with a PhosphoImager (Molecular Imager System GS 363, Bio-Rad) and the Molecular Analyst 2.1 software package.
27. Labeled *trp* leader RNA was synthesized according to the Riboprobe in vitro transcription system (Promega), as described previously (*4*), except that 100 μCi = 3.7 MBq of [α-^{33}P]UTP (3000 Ci/mmol) was used. Reaction mixtures contained 40 mM tris-HCl pH 8, 250 mM KCl, 4 mM $MgCl_2$, 20 units RNasin, and 0.5 mM L-tryptophan. Various concentrations of TRAP and AT were added, and the mixtures were incubated 10 min at room temperature, then 1.75 nM labeled RNA was added to a final volume of 10 μl, and the mixtures were reincubated 10 min at room temperature. The samples were electrophoresed on a 6% native polyacrylamide gel in 0.5× tris-borate EDTA at 4°C. RNA bands were quantified as in the in vitro transcription attenuation assay.
28. Cross-linking experiments with glutaraldehyde followed a published procedure (*11*). Reaction mixtures contained 0.75 μg of TRAP and/or 1.2 μg of AT in the presence or absence of 0.5 mM L-tryptophan in 20 mM NaCl, 4 mM $MgCl_2$. After incubating at room temperature for 20 min, glutaraldehyde (0.5 μl of 8%, w/v) was added and allowed to cross-link for 5 min at room temperature. Reactions were terminated by adding SDS sample buffer and boiling for 1 min. Samples were analyzed by 4 to 20% gradient SDS–polyacrylamide gel electrophoresis and protein bands were visualized by silver staining.
29. C. V. Hall, C. Yanofsky, *J. Bacteriol.* **151**, 918 (1982).
30. See www.ebi.ac.uk/~michele/jalview.

31. We are grateful to P. Gollnick for purified *B. subtilis* TRAP. We thank F. Gong, J. Sarsero, and M.-C. Yee for valuable technical advice, and we thank the Stanford PAN Facility for performing the mass spectrometry analyses. We are also grateful to P. Babitzke and P. Gollnick for critical reading of the manuscript. These studies were supported by grants from NIH and NSF.

2 May 2001; accepted 12 July 2001

REPORTS

Experimental Realization of Noiseless Subsystems for Quantum Information Processing

Lorenza Viola,[1]*† Evan M. Fortunato,[2]* Marco A. Pravia,[2] Emanuel Knill,[1] Raymond Laflamme,[1] David G. Cory[2]

We demonstrate the protection of one bit of quantum information against all collective noise in three nuclear spins. Because no subspace of states offers this protection, the quantum bit was encoded in a proper noiseless subsystem. We therefore realize a general and efficient method for protecting quantum information. Robustness was verified for a full set of noise operators that do not distinguish the spins. Verification relied on the most complete exploration of engineered decoherence to date. The achieved fidelities show improved information storage for a large, noncommutative set of errors.

Quantum information is represented in terms of superposition states of elementary two-level systems, known as qubits. The coherence properties of such superpositions are essential to the extraordinary capabilities that quantum mechanics promises for quantum simulation (*1*), computation (*2*), and communication (*3*). At the same time, they are also extremely vulnerable to the decoherence processes that real-world quantum devices undergo due to unwanted couplings with their surrounding environment (*4*). Thus, achieving noise control is indispensable for practical quantum information processing (QIP). While a variety of strategies have been devised to meet this challenge, no single method can compensate for a completely arbitrary noise process. Rather, constructing a reliable QIP scheme depends crucially on the errors that happen. If the interaction with the environment is sufficiently weak, then, to a good approximation, a restricted set of errors dominates the information loss, and active quantum error correction (QEC) (*5*) can be successfully implemented. Another instance where the relevant errors are a subset of all possible errors occurs when the system-environment interaction, no matter how strong, exhibits a symmetry. This motivated passive noise control schemes based on encoding quantum information into "noiseless" (or "decoherence-free", DF) subspaces (*6–9*). A DF subspace is spanned

by states of the system that, up to a possible common phase factor, experience no evolution under the noise. In fact, the existence of such invariant states is only one of the possibilities by which the underlying symmetry may reflect into the evolution of the system, i.e., the one where all the properties defining the quantum state are effectively conserved. While this turns out to be an exceptionally favorable situation, symmetries always imply the existence of conserved quantities. The notion of a noiseless subsystem (NS) (*10*) captures this intuition, opening the way for exploiting symmetries in full generality. The basic insight is that protecting quantum information need not require protecting the entire state. A classical example is parity preservation under the action of paired bit-flips, where the sum (modulo 2) of a bit string is unchanged by flips of any two bits. Similarly, by encoding quantum information into the abstract subsystems corresponding to preserved degrees of freedom, noiselessness is guaranteed even if errors still evolve the overall system's state.

The fact that NSs cover the full range of possibilities for error-free storage has immediate practical significance: Not only can NSs exist in the absence of DF subspaces, as in the situation addressed by our experiment, but they can ensure the same degree of protection through more efficient encodings (*10*). Even in a scenario where memory resources are not a concern, NSs allow for a major conceptual advance in realizing noise control in QIP. The identification of appropriate NSs provides the key for linking passive stabilization schemes with active error control based on either QEC or quantum error suppression (*11*), resulting in a unified picture of noise control strategies that is not achievable in terms of subspaces alone (*10*–*12*). In particular, although a correspondence exists between degenerate QEC codes and DF subspaces (*13*), establishing a similar duality for arbitrary codes requires the more powerful NS formalism (*10*, *12*, *14*). In fact, the deepest implication behind the NS idea is to point to the ultimate structure, a logical subsystem, where quantum information can reside. While the full impact of subsystems in QIP is still to be appreciated, this is likely to be substantially beyond noise protection itself—shedding light, for instance, on approaches to quantum universality (*15*) and entanglement (*16*).

A relevant symmetry arises when the environment couples to the qubits without distinguishing between them. This "far field" regime, where each qubit "feels" the same fluctuation, is entered whenever the spatial separations between the qubits are small relative to the correlation length of the environment. The resulting "collective" noise behavior provides the paradigmatic situation for discussing passive noise control. Experimental efforts to date have been limited to demonstrating the existence of protected subspaces under special types of collective noise—a single DF state of two photons (*17*) and a DF subspace of two trapped ions (*18*). For arbitrary collective noise acting on three qubits there are no protected subspaces, but there is a NS. Here, we realize this minimal, three-qubit NS to guarantee the preservation of one qubit against the most general collective noise.

Our physical system is composed of three spin 1/2 particles. Let $\sigma_\alpha^{(j)}$, $\alpha = x, y, z$, denote Pauli spin operators acting on the jth qubit, $j = 1, 2, 3$. Under collective noise conditions, only global angular momentum operators $S_\alpha = (\sigma_\alpha^{(1)} + \sigma_\alpha^{(2)} + \sigma_\alpha^{(3)})/2$ contribute to the system-environment interaction. If the spins are initially in a pure state ϱ_{in}, the effect of the environment may be depicted in terms of a quantum operation that leaves them in a mixed state, $\varrho_{in} \rightarrow \varrho_{out} = \mathcal{E}(\varrho_{in}) = \sum_a E_a \varrho_{in} E_a^\dagger$, for a set of error operators $\{E_a\}$ satisfying $\sum_a E_a^\dagger E_a = \mathbb{1}$. The possible errors that the error generators S_α can induce belong to the "interaction algebra" $\mathcal{A}$ (*10*), which contains all the linear combinations of arbitrary products of S_α and the identity. In the weak-noise limit addressed by ordinary QEC, the relevant first-order errors essentially coincide with the generators S_α. Error operators involving products of any number of S_α occur for sufficiently strong or sufficiently long exposure to noise. Thus, $\mathcal{A}$ provides the appropriate tool for discussing protection of information with "infinite-distance," against arbitrarily large noise strength and/or order in time. The interaction algebra $\mathcal{A}_c$ for general collective noise consists of all the totally symmetric operators—which reflects the permutation-symmetry of the noise. For three qubits, the dimension of the symmetric operators' subspace is 20, so an error basis for describing an arbitrary collective noise process can be constructed from 20 three-spin operators (out of the possible 64). Simpler collective noise models, like the ones probed in (*17*, *18*), correspond to smaller error algebras. For instance, collective dephasing with arbitrary strength, $\mathcal{E}_z$, is described by an abelian subalgebra $\mathcal{A}_z$ spanned by four elements, $\mathbb{1}$, S_z, S_z^2, S_z^3—and similarly for any fixed axis. The full, nonabelian $\mathcal{A}_c$ can be induced by cascading noise processes along at least two noncommuting spatial directions, e.g., $\varrho_{out} = \mathcal{E}_{zx}(\varrho_{in}) = \mathcal{E}_z(\mathcal{E}_x(\varrho_{in}))$.

The NS reported here lives in the four-dimensional subspace $\mathcal{H}_{1/2}$ of states carrying total angular momentum $S = 1/2$ (*10*, *19*). Basis states for $\mathcal{H}_{1/2}$ are specified by two quantum numbers, $|\lambda, s_z\rangle$, where $s_z = \pm 1/2$ is the eigenvalue of S_z, and $\lambda = 0,1$ accounts for the existence of two distinct pathways leading to total angular momentum $S = 1/2$ (*14*, *19*). Because each of the error generators S_α acts equivalently and nontrivially only within each path, the quantum number λ is preserved under the action of arbitrary errors in $\mathcal{A}_c$. Thus, the logical subsystem L supported by λ is a NS under general collective noise. In other words, $\mathcal{H}_{1/2}$ can be pictured as the state space of two abstract qubits: L, which is fully protected against collective errors, and Z, which carries all the entropy inserted by the noise. The stability of information encoded in L against all error operators in $\mathcal{A}_c$ characterizes L as an infinite-distance QEC code for collective noise (*10*). Because four physical qubits are required for attaining the same goal through a DF subspace (*6*), the three-qubit NS realizes the smallest one-bit noiseless quantum memory under $\mathcal{A}_c$.

In terms of the single-qubit input ρ_{in} and output ρ_{out} for the data spin alone (see Fig. 1 for outline of experiment), the overall effect of the procedure is described by a one-bit quantum operation that maps $\rho_{in} \rightarrow \rho_{out} = \mathcal{Q}(\rho_{in})$. Ideally, $\rho_{out} = \rho_{in}$. In the presence of unavoidable imperfections, we invoke the entanglement fidelity F_e (*20*) as the appropriate measure for quantifying the preservation of the quantum data. For a given process $\mathcal{Q}$, $F_e(\mathcal{Q}) = 1$ if and only if $\mathcal{Q}$ perfectly preserves every input state. A complete characterization of $\mathcal{Q}$ from experimentally available data can be obtained by "quantum process tomography" (*21*), which relies on measuring the output states generated from a complete set of independent input states. Let $|0\rangle$ and $|1\rangle$ denote the eigenstates of σ_z, and define $|+\rangle = (|0\rangle + |1\rangle)/\sqrt{2}$, $|+i\rangle = (|0\rangle + i|1\rangle)/\sqrt{2}$, respectively. Under the assumption that $\mathcal{Q}$ describes a "unital" process for which $\mathcal{Q}(\mathbb{1}) = \mathbb{1}$, $F_e(\mathcal{Q})$ can be calculated as (*22*)

$$F_e(\mathcal{Q}) = (F_{|0\rangle} + F_{|+\rangle} + F_{|+i\rangle} - 1)/2$$

where $F_{|\psi_{in}\rangle} = Tr\{|\psi_{in}\rangle\langle\psi_{in}|\mathcal{Q}(|\psi_{in}\rangle\langle\psi_{in}|)\}$ is the input-output fidelity for the intended one-bit pure input state $|\psi_{in}\rangle$.

Our implementation was performed by liquid-state nuclear magnetic resonance (NMR) on a sample of ^{13}C-labeled alanine (Fig. 2) in D_2O solution, with a 300-MHz Bruker Avance spectrometer. NMR QIP has been extensively discussed in the literature (*23*). Room-temperature NMR qubits exist in highly mixed, separable states. Thus, NMR QIP relies on "pseudo-pure" (p.p.) states whose traceless (or "devia-

[1]Los Alamos National Laboratory, Los Alamos, NM 87545, USA. [2]Department of Nuclear Engineering, Massachusetts Institute of Technology, Cambridge, MA 02139, USA.

*These authors contributed equally to this work.
†To whom correspondence should be addressed. E-mail: lviola@lanl.gov

tion") component is proportional to that of the corresponding pure state. The identity component of the density matrix is unobservable and can be treated as a constant under the assumption of unital dynamics (*24*). Initialization of the qubits in one of the 3-spin p.p. input states $\varrho_{in}^{p.p.} = |00\psi_{in}\rangle\langle 00\psi_{in}|$, where the data-bit state $|\psi_{in}\rangle = |0\rangle, |+\rangle, |+i\rangle$ is defined above, was accomplished with standard gradient-pulse techniques. A sequence of transformations generating the above states from the 3-spin thermal equilibrium state, as well as other implementation details, can be found in (*25*). State preparation was verified by tomographically reconstructing the resulting 3-spin deviation density matrix. An amount of identity component able to optimize the fidelity with the intended 3-spin p.p. state was added to the experimental $\varrho_{in}^{p.p.}$ (*26*) and maintained throughout the analysis. The evolution of a p.p. state is equivalent to the corresponding pure-state evolution under unital dynamics. The logical manipulations involved in the NS encoding and decoding were mapped into ideal pulse sequences by standard quantum network methods (*23*). Pulses were implemented by modulating the internal Hamiltonian of the alanine molecule (Fig. 2) with externally controlled radio-frequency (RF) magnetic fields.

To investigate the NS performance in a controlled way, the time delay between encoding and decoding is designed to implement a net evolution of the spins under a desired collective noise model. Unwanted, symmetry-breaking dynamics generated by the molecule's internal Hamiltonian were refocused by using standard average Hamiltonian techniques (*23*). A variety of collective noise processes can be engineered through gradient-diffusion methods (*27*, *28*). A pulsed magnetic field gradient $\partial B_z/\partial z$ parallel to the static quantizing field B_z causes the spins to precess with a z-dependent Zeeman rate, thereby acquiring a phase factor that is identical for each species but varies linearly with z (*29*). These spatially dependent phases add incoherently to zero when the integrated signal from the sample is measured. Thus, the action of a strong gradient pulse over the ensemble amounts to an incoherent implementation of all the possible collective phase errors, emulating the error algebra $\mathcal{A}_z$ of the strong dephasing regime. Collective noise along an arbitrary axis is induced by sandwiching a z-noise between RF pulses, effecting a collective rotation of the spin state to the desired axis (*28*). The incoherent action of a single gradient pulse could be refocused by a second inverse gradient. A truly irreversible, decoherent implementation of collective noise is obtained by allowing for molecular diffusion to take place for a time Δt before applying an inverse gradient. Because the molecules have moved, the spins' phases are not returned to their original values but are randomly modified. Thus, the combined gradient-diffusion action results in an exponential signal loss whose effective decay rate $1/\tau$ is proportional to the diffusion constant and tunable with the gradient intensity (*27*).

Decoherent collective noise of variable strength was engineered by stepping the gradient amplitude from 0 to the maximum achievable value of about 0.5 T/m, and applied for a fixed evolution time t_{ev}. All noise strengths $1/\tau$ were calibrated by independent measurements with a gradient stimulated echo sequence (*27*). The attained ratios t_{ev}/τ are sufficient to push the evolution beyond the weak-dephasing regime that can be compensated for by QEC (*30*). Separate experiments were performed to expose the NS-encoded qubit and the unencoded data spin, C_3, to single-axis collective z and y noise (Fig. 3). Both the unencoded and NS-encoded data are fit to a decaying exponential model, $F_e = A_1 \exp(-t_{ev}/\tau) + B$ (*31*). The asymptotic F_e value given by B is a relevant figure of merit for lower-bounding the entanglement fidelity attainable for single-axis noise of arbitrary strength. The test data are expected to decay under a single-qubit dephasing channel along y—i.e., $A_1 = B = 0.50$—as opposed to the observed values of $A_1 = 0.51 \pm 0.04$, $B = 0.43 \pm 0.03$. For the NS data, the theory predicts a constant unit F_e.

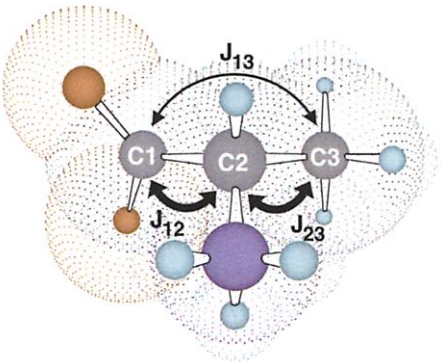

Fig. 2. Molecular structure of ^{13}C-labeled alanine. The internal Hamiltonian for the three carbon qubits is accurately described by $H_{int} = \pi[\nu_1\sigma_z^{(1)} + \nu_2\sigma_z^{(2)} + \nu_3\sigma_z^{(3)} + (J_{12}\sigma_z^{(1)}\sigma_z^{(2)} + J_{23}\sigma_z^{(2)}\sigma_z^{(3)} + J_{13}\sigma_z^{(1)}\sigma_z^{(3)})/2)]$. The resonance frequency of carbon-13 nuclei in a magnetic field of ~ 7.2 T is $\nu_0 = 75.4736434$ MHz. The chemical shifts and the J-coupling parameters are as follows: $\nu_1 - \nu_0 = 7167$ Hz, $\nu_2 - \nu_0 = -2286.5$ Hz, $\nu_3 - \nu_0 = -4881.4$ Hz, $J_{12} = 54.1$ Hz, $J_{23} = 35.0$ Hz, and $J_{13} = -1.3$ Hz. Conditional gates between qubits 1 and 3 were replaced by compositions of operations between pairs (1,2), (2,3) to avoid using the slow (1,3)-coupling. Once the logical operations were translated into sequences of RF pulses and delays, complete pulse programs for U_{enc}, U_{dec} resulted from the compilation of the partial pulse programs for individual gates. Consecutive pulses were combined whenever possible to allow for a faster implementation. The pulses were designed to guarantee self-refocusing of all the J-coupling and chemical-shift evolutions.

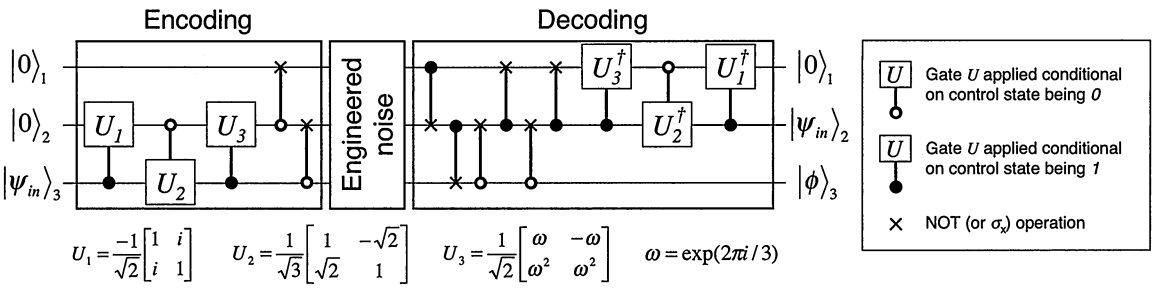

Fig. 1. Logical quantum network for the NS experiment. The information is initially stored in qubit 3, while qubits 1 and 2 are initialized in the state $|0\rangle$. A unitary encoding transformation U_{enc} is applied to map the initial input state space into the NS (*19*). A time delay follows, during which the qubits are stored in the NS memory. Applying the unitary transformation U_{dec} returns the information to the state of carbon 2. Encoding and decoding networks are expressed in terms of controlled rotations. U_{enc} is a simplified version of U_{dec}^{-1} obtained by exploiting the knowledge of the initial non–data bits. For $|\psi_{in}\rangle = \alpha|0\rangle + \beta|1\rangle$ with arbitrary complex α, β, $|\alpha|^2 + |\beta|^2 = 1$, and an initial 3-spin state $|0\rangle_1 \otimes |0\rangle_2 \otimes |\psi_{in}\rangle_3 = |00\psi_{in}\rangle$, U_{enc} implements a transformation $U_{enc}|00\psi_{in}\rangle = |\psi_{in}\rangle_L \otimes |-1/2\rangle_Z$. A collective noise process $\mathcal{E}_{coll} = \{E_a\}$ only affects the Z subsystem. U_{dec} decodes a generic noisy state $E_a(|\psi_{in}\rangle_L \otimes |-1/2\rangle_Z)$ in $\mathcal{H}_{1/2}$ to the computational basis, $U_{dec}[(\alpha|0\rangle_L + \beta|1\rangle_L) \otimes (c_a|-1/2\rangle_Z + d_a|+1/2\rangle_Z)] = \alpha c_a|000\rangle + \beta c_a|010\rangle + \alpha d_a|001\rangle + \beta d_a|011\rangle$ for appropriate coefficients. This produces the intended state of qubit 2 upon discarding spins 1 and 3, i.e., $\mathrm{Tr}_{1,3}\{U_{dec}[\mathcal{E}_{coll}(|\psi_{in}\rangle_L\langle\psi_{in}| \otimes |-1/2\rangle_Z\langle -1/2|)]U_{dec}^\dagger\} = |\psi_{in}\rangle_2\langle\psi_{in}|$.

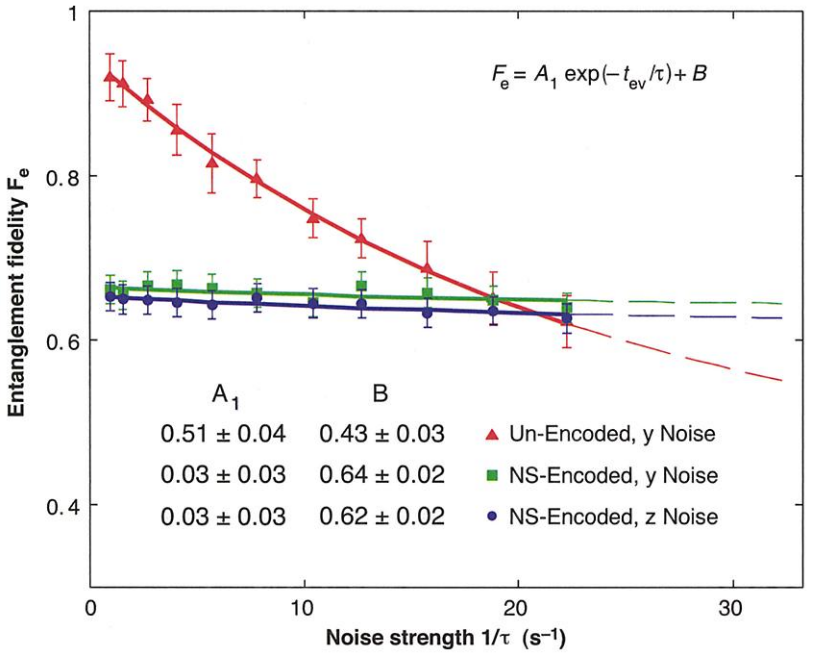

Fig. 3. Experimentally determined entanglement fidelities for the decoherent implementation of single-axis collective error models. We used a diffusion time $\Delta t \sim 34$ ms and gradient times $\delta \sim 5$ ms, giving a fixed $t_{ev} = 2\delta + \Delta t \sim 44$ ms. Variable-strength collective noise along either the y axis [NS-encoded (squares) and un-encoded data (triangles)] or the z axis [NS-encoded data only (circles)] was applied during t_{ev}. The decay of the un-encoded spin, C_3, was measured by turning off the NS-encoding and -decoding sequences. Both the un-encoded and encoded data are fit to an exponential decay, with the interpolated (solid) and extrapolated (dashed) lines shown in the plot. Best estimates and standard deviations of the parameters are also given. The relatively large error bars of the data arise from a conservative estimate of the uncertainties associated with the noise-strength determination.

Table 1. Summary of experimental data for the incoherent implementation of various collective error models. The first column lists the one-bit quantum processes realized in the experiment. Gradient fields with maximum strength ~ 0.5 T/m were applied during a fraction $\delta \sim 0.5$ ms of the evolution period, $t_{ev} \sim 3$, 6, 9 ms for single-, double-, and triple-axes error models, respectively. In addition to the applied error model $\mathcal{E}_x$, $\mathcal{E}_y$, $\mathcal{E}_z$, $\mathcal{E}_{zx}$, $\mathcal{E}_{zy}$, and $\mathcal{E}_{yzx}$, the channel label specifies whether (ns) or not (un) encoding and decoding procedures were implemented. The processes $\mathcal{Q}_{0,ns}$, $\mathcal{Q}_{00,ns}$, and $\mathcal{Q}_{000,ns}$ differ in the length of the evolution period over which they apply the trivial error model (i.e., the identity evolution). For each process, the input-output fidelities $F_{|\psi_{in}\rangle}$ involved in the process tomography as well as the resulting entanglement fidelities F_e are listed. Statistical uncertainties are ~ 2%, arising from errors in the tomographic density matrix reconstruction.

Quantum process	$F_{\|0\rangle}$	$F_{\|+\rangle}$	$F_{\|+i\rangle}$	F_e
$\mathcal{Q}_{x,un}$	0.50	0.97	0.49	0.48
$\mathcal{Q}_{0,ns}$	0.84	0.74	0.78	0.68
$\mathcal{Q}_{x,ns}$	0.79	0.74	0.78	0.66
$\mathcal{Q}_{y,ns}$	0.81	0.77	0.82	0.70
$\mathcal{Q}_{z,ns}$	0.86	0.72	0.76	0.67
$\mathcal{Q}_{zx,un}$	0.49	0.50	0.50	0.24
$\mathcal{Q}_{00,ns}$	0.80	0.79	0.80	0.70
$\mathcal{Q}_{zx,ns}$	0.78	0.80	0.82	0.70
$\mathcal{Q}_{zy,ns}$	0.79	0.80	0.82	0.70
$\mathcal{Q}_{000,ns}$	0.77	0.79	0.78	0.67
$\mathcal{Q}_{yzx,ns}$	0.75	0.80	0.77	0.66

In the experiment, both a constant term, $B = 0.64 \pm 0.02$ (y) and $B = 0.62 \pm 0.02$ (z), and a small decaying contribution, $A_1 = 0.03 \pm 0.03$ (both y and z), are seen. For both the NS- and the unencoded cases, departures from the ideal values are explained by pulse imperfections and by natural relaxation processes, whose action is assumed to be independent of the applied-noise strength. Several remarks are in order concerning the NS data. First, the fact that A_1 is compatible with zero suggests that the measured signal predominantly originates from the NS, as a signal from other locations would decay with increasing applied noise. Second, because B well exceeds the threshold value of 0.50, the implementation guarantees, in principle, entanglement preservation for arbitrary noise strength (*32*). Finally, the fidelities achieved for sufficiently strong noise imply an actual improvement in preserving quantum information via the NS code.

A variety of incoherent collective error processes were also implemented to explore exhaustively the NS robustness under strong single- and multiple-axes noise that fully probe the nonabelian error algebra of general collective noise. Incoherent implementations have the advantage that full-strength error models can be induced quickly as compared with the natural relaxation time scales. The experimental data for both unencoded and NS-encoded evolutions are summarized in Table 1. As in the decoherent case, the F_e values for single-axis noise, $\mathcal{E}_\alpha$, $\alpha = x, y, z$, demonstrate the infinite error-correcting behavior of the NS code against errors in the corresponding abelian subalgebra $\mathcal{A}_\alpha$. Robustness against the full $\mathcal{A}_c$ is verified through the composite processes ($\mathcal{Q}_{zx}$, $\mathcal{Q}_{zy}$, $\mathcal{Q}_{yzx}$) obtained by sequentially implementing evolution periods corresponding to single-axis error models along different directions. The measured input-output and entanglement fidelities are consistent with the expectation that single-axis and composite noise processes induce full phase-damping and full depolarization on the unencoded data bit—with predicted fidelities of 0.50 and 0.25, respectively. Infinite-distance error-correcting behavior with respect to $\mathcal{A}_c$ is established by the unchanged fidelity levels observed in the presence of the applied noise relative to the corresponding no-error case. The data show a substantial increase in the amount of information retained under the action of the applied error models.

NSs provide extremely efficient means of preserving quantum information whenever a dominant symmetry occurs in the noise. Therefore, symmetry should be a leading criterion for engineering QIP. We have shown that the implementation of NSs is within the reach of current quantum information technologies. Although the attained fidelities are less than ideal and point to the need for improved quantum control capabilities, our implementation convincingly demonstrates improvement in error-correcting a class of both abelian and nonabelian error models via an infinite-distance one-qubit quantum code. The encoding, decoding, and verification techniques used here are exportable to other quantum information devices, where the dominant noise mechanisms are collective in nature. Besides providing the chief source of ambient noise in trapped ion QIP (*18*), collective noise behavior is also expected to be predominant in solid-state architectures based on either nuclear spin (*33*) or quantum dot (*34*) arrays. NS coding, possibly combined with fault-tolerant and active control methods, can thus play a practical role for both reliable storage and manipulation of quantum information in future QIP.

References and Notes

1. S. Lloyd, *Science* **273**, 1073 (1996).
2. C. H. Bennett, D. P. DiVincenzo, *Nature* **406**, 247 (2000).
3. C. H. Bennett, P. W. Shor, *IEEE Trans. Inf. Theory* **44**, 2724 (1998).

4. W. H. Zurek, *Phys. Today* **40** (no. 10), 36 (1991).
5. J. Preskill, *Proc. R. Soc. London Ser. A* **454**, 385 (1998).
6. P. Zanardi, M. Rasetti, *Phys. Rev. Lett.* **79**, 3306 (1997).
7. L.-M. Duan, G.-C. Guo, *Phys. Rev. Lett.* **79**, 1953 (1997).
8. D. A. Lidar, I. L. Chuang, K. B. Whaley, *Phys. Rev. Lett.* **81**, 2594 (1998).
9. D. A. Lidar, D. Bacon, J. Kempe, K. B. Whaley, *Phys. Rev. A* **63**, 022306 (2001).
10. E. Knill, R. Laflamme, L. Viola, *Phys. Rev. Lett.* **84**, 2525 (2000).
11. L. Viola, E. Knill, S. Lloyd, *Phys. Rev. Lett.* **85**, 3520 (2000).
12. P. Zanardi, *Phys. Rev. A* **63**, 012301 (2001).
13. D. A. Lidar, D. Bacon, K. B. Whaley, *Phys. Rev. Lett.* **82**, 4556 (1999).
14. J. Kempe, D. Bacon, D. A. Lidar, K. B. Whaley, *Phys. Rev. A* **63**, 042307 (2001).
15. D. P. DiVincenzo, D. Bacon, J. Kempe, G. Burkard, K. B. Whaley, *Nature* **408** (2000).
16. P. Zanardi, *Phys. Rev. Lett.* **87**, 077901 (2001).
17. P. G. Kwiat, A. J. Berglund, J. B. Altepeter, A. G. White, *Science* **290**, 498 (2000).
18. D. Kielpinski *et al.*, *Science* **291**, 1013 (2001); published online 5 January 2001 (10.1126/science.1057357).
19. L. Viola, E. Knill, R. Laflamme, *J. Phys. A* **34**, 7067 (2001).
20. B. Schumacher, *Phys. Rev. A* **54**, 2614 (1996).
21. I. L. Chuang, M. A. Nielsen, *J. Mod. Opt.* **44**, 2455 (1997).
22. M. A. Nielsen, E. Knill, R. Laflamme, *Nature* **396**, 52 (1998).
23. D. G. Cory *et al.*, *Fortschr. Phys.* **48**, 875 (2000).
24. We explicitly verified this assumption by tomographically reconstructing the super-operator corresponding to the process $\mathcal{Q}_{0,ns}$ (see Table 1 for definition). We found a maximum absolute deviation from identity, $|\mathbb{1} - \mathcal{Q}_{0,ns}(\mathbb{1})| \sim 4\%$.
25. G. Teklemariam, E. M. Fortunato, M. A. Pravia, T. F. Havel, D. G. Cory, *Phys. Rev. Lett.* **86**, 5845 (2001).
26. Optimization of the fidelity with respect to the intended 1-spin p.p. state for the data carbon alone results in an amount of identity component that is equal to the one based on the corresponding 3-spin p.p. state within the experimental accuracy.
27. A. Sodickson, D. G. Cory, *Prog. Nucl. Magn. Res. Spectrosc.* **33**, 77 (1998).
28. T. F. Havel, Y. Sharf, L. Viola, D. G. Cory, *Phys. Lett. A* **280**, 282 (2001).
29. For a given species, e.g., ^{13}C, the gradient action is symmetric to an accuracy better than 0.1%. By contrast, dephasing processes naturally occurring in alanine are dominated by noncollective effects reflecting the different chemical environment of each carbon.
30. D. G. Cory *et al.*, *Phys. Rev. Lett.* **81**, 2152 (1998).
31. We initially fit the data to a multiexponential model, $F_e = \Sigma_n A_n \exp(-n^2 t_{ev}/\tau) + B$, that accounts for the possible single, double, and triple (n = 1, 2, 3) decay modes of quantum coherences in a 3-spin system. From the resulting best estimates we confirm that contributions from double (A_2) and triple (A_3) quantum coherence terms, arising from unintentionally populated states outside $\mathcal{H}_{1/2}$, are negligibly small.
32. C. H. Bennett, D. P. DiVincenzo, J. A. Smolin, W. K. Wootters, *Phys. Rev. A* **54**, 3824 (1996).
33. B. E. Kane, *Nature* **393**, 133 (1998).
34. P. Zanardi, F. Rossi, *Phys. Rev. Lett.* **81**, 4752 (1998).
35. This work was supported by the National Security Agency and Advanced Research and Development Activity (Army Research Office contract DAAD19-01-1-0519), by the Defense Sciences Office of the Defense Advanced Research Projects Agency (contract MDA972-01-1-0003), and by the Department of Energy (contract W-7405-ENG-36). We thank G. Teklemariam and N. Boulant for help with implementation, and G. Boutis, R. Onofrio, T. Havel, and S. Lloyd for valuable discussions.

8 May 2001; accepted 15 August 2001

Direct Measurement of the Preferred Sense of NO Rotation After Collision with Argon

K. Thomas Lorenz,[1] David W. Chandler,[1] James W. Barr,[2] Wenwu Chen,[2] George L. Barnes,[2] Joseph I. Cline[2]

The preferred sense of product molecule rotation (clockwise or counterclockwise) in a bimolecular collision system has been measured. Rotationally inelastic collisions of nitric oxide (NO) molecules with Ar atoms were studied by combining crossed molecular beams, circularly polarized resonant multiphoton ionization probing, and velocity-mapped ion imaging detection. The observed sense of NO product rotation varies with deflection angle and is a strong function of the NO final rotational state. The largest preferences for sense of rotation are observed at the highest kinematically allowed product rotational states; for lower rotational states, the variation with deflection angle becomes oscillatory. Quantum calculations on the most recently reported NO-Ar potential give good agreement with the observed oscillation patterns in the sense of rotation.

Crossed molecular beam studies of inelastic and reactive bimolecular collisions have provided the most detailed information on the elementary processes fundamental to an understanding of chemical reactions (*1*, *2*). The power of the crossed beam experiment arises from the control of initial conditions such as collision energy and the direction of reactant approach. Scalar quantities measured in such experiments include chemical reaction probabilities and energy partitioning among product states. Measurements of vector quantities, such as product velocity or rotational angular momentum, reveal the correlations among the directional properties of the reactant and product trajectories. The vector quantity measured in traditional crossed beam experiments is the differential cross section (DCS), which gives the probability of product formation as a function of the angle between the directions of product approach and reactant recoil. Recent advances have made possible the measurement of product recoil direction in coincidence with the direction of product angular momentum. Such measurements provide a detailed picture of the final reaction trajectory, which is highly sensitive to the topology of the potential energy surface (PES) along the reaction pathway.

Case and Herschbach have shown that measurements of four vectors provide a complete account of the scattering dynamics of an atom-diatom system (*3*). The important vectors are $\mathbf{v}$, $\mathbf{v}'$, $\mathbf{j}$, and $\mathbf{j}'$, which describe the reactant and product relative velocity and the reactant and product angular momentum, respectively (*3*–*5*). If the reactant diatom is nonrotating, then the angular correlation among the directions of reactant approach $\mathbf{v}$, product ejection $\mathbf{v}'$, and product angular momentum $\mathbf{j}'$ is of interest. The full $\mathbf{v}$-$\mathbf{v}'$-$\mathbf{j}'$ correlation includes both rotational alignment (the preferred plane of product rotation) and the rotational orientation (the preferred sense of product rotation) with respect to the scattering plane defined by $\mathbf{v}$ and $\mathbf{v}'$. Recent advances in Doppler spectroscopy (*6*, *7*), laser ionization/time-of-flight techniques (*8*–*10*), and ion imaging (*11*, *12*) have made possible experimental measurements of rotational alignment for a number of reactive and inelastic scattering systems. However, theoretical studies have indicated that rotational orientation may be a more sensitive probe of the scattering dynamics (*13*–*15*). In this paper, we report the first experimental observations of molecular rotational orientation in a full two-body collision.

Our experiments study rotationally inelastic collisions of nonrotating, nonvibrating, ground-electronic-state NO molecules with Ar atoms [NO $^2\Pi_{1/2}(v = 0, j = 1/2)$ + Ar → NO $^2\Pi_{1/2}(v' = 0, j')$ + Ar] at a center-of-mass (CM) frame collision energy of 66 meV. The highest NO rotational state that can be populated at this collision energy is $j' = 16.5$. Figure 1 shows a schematic representation of one type of trajectory for classical scattering superimposed over image data described below. The NO molecule, tilted by an angle α, approaches from the right with initial velocity $\mathbf{v}$. The Ar atom approaches from the left, offset by impact parameter b. After collision, the initial NO velocity, $\mathbf{v}$, is deflected through the angle θ. For simplicity in this illustration, we have chosen the reactant NO internuclear axis to lie in the scattering plane, so that the product NO angular momentum

[1]Combustion Research Facility, Post Office Box 969, MS9055, Sandia National Laboratory, Livermore, CA 94550, USA. [2]Department of Chemistry and Chemical Physics Program, University of Nevada, Reno, NV 89557, USA.